EAI Endorsed Transactions
on Pervasive Health and Technology
Research Article EAI.EU

Biomorphic Design of Age-Friendly Wearable Devices: Flexible Circuits and Self-Luminescent Display Interfaces Based on Vascular Bionic Structures

Yingyu Zhang[1,*]

[1]Department of Changchun Humanities, University of Changchun, Changchun 130022, China

Abstract

With the accelerating aging of the global population, the importance of health monitoring and assistive technologies for the elderly is becoming increasingly prominent. This study aims to propose and validate a biomorphic design framework based on vascular biomimetic structures to address the challenges of mechanical adaptability, signal stability, and cognitive interaction in age-friendly wearable devices. Using microfluidic lithography and differential capillary self-assembly, a liquid metal flexible circuit with a fractal topology mimicking human microvasculature is constructed on a SEBS/TPU composite substrate. A biomimetic microhinge array is used to disperse stress, and micropits are laser-engraved on the surface to enhance breathability. The display interface, based on a poly(3,4-ethylenedioxythiophene) microcapsule array, combines electrochromic and photoluminescent effects to map parameters such as blood pressure and blood oxygen into dynamic fractal growth patterns. Experimental data show that the biomimetic circuit exhibits a resistance change of only 11.72% under a strain of only 15%, and the substrate stiffness pressure is 0.82±0.07 kPa, ensuring signal stability and comfortable wear during exercise. The user experience is significantly improved, with a low discomfort feedback rate of 7.2%. The conclusion shows that biomorphic design based on vascular bionic structure provides a suitable and systematic solution for the physiological adaptation and cognitive interaction of elderly-friendly wearable devices.

Keywords: Vascular Bionics; Flexible Circuits; Self-Luminous Displays; Biomorphic Design; Age-Friendly Wearable Devices

Received on 10 December 2025, accepted on 12 December 2025, published on 02 February 2026

doi: 10.4108/eetpht.11.11674

1. Introduction

No population is witnessing such an unprecedented transition as the aging of the global population. Most aged people prefer home care, which implies the importance of health monitoring and assistance technology for the elderly in order to deal with aging challenges. Continuous health monitoring, as one of the key capabilities of smart wearable devices, can be widely applied in various aspects of health management, ranging from heart rate and blood pressure monitoring to blood oxygen measurement and activity tracking. However, even though flexible electronics have become commonly used in recent years, conventional wearable devices still suffer from multiple limitations of age-friendly design: rigid circuits are uneven under skin deformation and therefore cause discomfort and signal distortion; display interfaces tend to deliver abstract data and cannot adapt to age-related cognitive decline; low-permeable materials easily trigger skin inflammation. Such problems arise from a lack of biocompatibility at their core, which requires rethinking about design paradigms through biomimicry.

This paper presents and validates a biomorphic design framework grounded in vascular bionic structures to address the age-friendly wearable device concerns of mechanical

*Corresponding author. Email: 1390372106@qq.com

adaptation, signal stability, and cognitive interaction. By mimicking the fractal topology of human microvasculature and the interlocking behavior of the devil ironclad beetle's microhinge, the device reaches synergistic mechanical and moisture permeability optimization through GaIn liquid metal infusion and SEBS/TPU composite substrate molding. A poly(3,4-ethylenedioxythiophene) microcapsule array is further constructed based on combined electrochromic and photoluminescent effects, thus mapping physiological parameters into intuitive, branched fractal growth patterns and improving the information recognition efficiency of elderly users. Finally, the interface layout is optimized according to ISO 7001 standards relevant to age-friendly wear as it integrates mid- and low-frequency voice alerts and promotes magnetic modularity to switch between wristband and chest patch modes. A micro-dimpled surface treatment reduces skin adhesion, significantly improving long-term wear comfort.

This paper is organized as follows: it reviews the current state of research in age-friendly design and wearable technology, clarifying the innovative positioning of biomorphic design; it elaborates on the methodological details of vascular biomimetic structure fabrication, flexible circuit integration, and display interface development; it quantifies the practical effectiveness of biomimetic design through electromechanical performance testing, physiological monitoring accuracy verification, and user experience evaluation; it discusses the theoretical implications of biomorphic design for the age-friendly paradigm, and summarizes the research conclusions and future directions.

2. Related Work

In the context of an aging society, age-friendly design has become an important topic in industrial design and health research. Phlix et al. [1] used qualitative research methods, including field observation, in-depth interviews, and participatory workshops, to conduct a case study in a super-diverse community to analyze the spatial usage experience and needs of elderly people of different ages and cultural backgrounds. The physiological and behavioral needs of elderly people in Chinese nursing homes for furniture have not been systematically studied, and existing furniture designs often fail to fully meet their actual usage conditions. Yun [2] proposed key parameters for furniture design based on the physiological decline characteristics of Chinese elderly people. The study clarified the safety, comfort, and functional requirements that age-friendly furniture should have, and provided specific suggestions for the design of furniture in nursing homes. In the context of an aging society, product design needs to systematically respond to the diverse needs of the elderly, but there is currently a lack of an integrated age-friendly product design system. Yongsheng and Xiaoqi [3] constructed a multi-level and multi-dimensional age-friendly product design system framework based on literature analysis and user surveys, covering the three levels of physiological, psychological, and social. In order to accurately identify and evaluate the core elements of the design of smart wearable devices for the elderly, Yang and Wu [4] proposed a design method for smart wearable devices for the elderly based on the structural equation model (SEM). They constructed a SEM model and conducted empirical analysis using SPSS 27.0 and AMOS 27.0 software. They obtained the influencing factors of 7 latent variables and 22 observable variables, and used standardized path analysis to obtain the weight values of each influencing factor. According to the weight values, the importance of each factor was determined, the design focus was clarified, and the design application was carried out. Liu et al. [5] summarized the characteristic changes of the elderly population in the three dimensions of physiological, psychological and social attributes from the human body layer; they analyzed and summarized the seven related development technologies of smart wearable devices suitable for the elderly, including sensors, materials, morphology, structure, interaction mode, functional algorithm and evaluation method; then, they sorted out the five functional systems of smart wearable devices for the elderly, including physiological system, nervous system, motor system, emotional system and spatial movement system. Furthermore, based on the development status of six related industries in the industrial ecology layer, they discussed the current design paradigm of smart wearable products for the elderly.

Against the backdrop of an increasingly aging society and a predominantly home-based elderly care model, Zhu et al. [6] studied and analyzed the theoretical concepts of artificial intelligence devices and the design of elderly-friendly home spaces, and the relationship between them. They also elaborated on the functional attributes and applicable spaces of different types of artificial intelligence devices. Secondly, they proposed practical suggestions for the specific application of artificial intelligence devices in various elderly-friendly functional spaces based on different spatial characteristics. Abraham et al. [7] explored how sensory deficits can confuse cognitive assessment results through a literature review and empirical data analysis, and proposed a cognitive research framework that integrates sensory assessment. They emphasized that sensory function assessment must be systematically incorporated into cognitive aging research to avoid misjudging cognitive abilities and promote a more comprehensive elderly health research paradigm. Thomas Tobin et al. [8] used an intersectional theoretical framework to review existing minority aging research and analyzed how multiple identities affect health outcomes and research participation. They called for the use of intersectional methods in aging research to more comprehensively understand the complex needs of minority elderly people and promote health equity. There is a disconnect between aging research and health equity. Gilmore-Bykovskyi et al. [9] combined community participatory research (CBPR) to promote more inclusive and ethical elderly research practices. Carr et al. [10] explored the types of motivations for participating in aging research and their predictive factors. The study found that there are many types of motivations for participating in aging research, including personal interests, career development, social

responsibility, etc. The motivation types discussed in this article correspond to the personal history, working sector, and setting views of the researcher. While the functional algorithms and interactive design of a smart wearable device have evolved from the traditional one, the research results concerning the biomorphic design of the device, particularly flexible circuits and self-luminous display technology, are still inadequate, and the systematic analysis is missing. The article takes a bionic approach and proposes a design mode for flexible circuits and self-luminous display interfaces based on vascular bionic structures. The objective is to provide new perspectives and technical references for the design of aging-friendly wearable devices.

3. Materials and Methods

3.1 Vascular Biomimetic Structures Design and Fabrication

The vascular biomimetic structure emulates the fractal topology and mechanical adaptability of human capillaries. Guided by a microfluidic environment, a three-dimensional branching network is established on a PDMS substrate using a photolithography-soft lithography process. The density of 1200 branches/cm² is inspired by the physiological distribution of microvessels in the dermis and ensures efficient conductive routes present within a limited space. To maximize the infusion of GaIn alloy, a differential capillary self-assembly technique is introduced. The hydrophilicity gradient on channel surfaces is manipulated to exert differential capillary forces, allowing the low-viscosity liquid metal to autonomously fill the micron-sized branches without creating air bubbles, thus improving the uniformity of the conductive network. The SEBS/TPU composite substrate counteracts the surface's mechanical properties, and through the synergy of borate and hydrogen bonds, it features a Shore A of 25 and high resilience. Lastly, structural biomimetics is inspired by the interlocking elliptical units of the devil ironclad elytra and grafts a micro-hinge array with a ratio of 1:1.8 between the vertical-horizontal length inside the base. Tensile stress is dispersed through multi-stage deformation. Under a 15% biaxial stretch, the micro-hinge array internally maintains the circuit's structural integrity. Lastly, the surface is laser-engraved with micro-pits (diameter 50μm, depth 20μm) to simulate the skin texture and increase breathability and reduce feelings of humidity during wear.

The optimization of the microfluidic architecture integrates the theory of the vascular fractal geometry. The fractal dimension D_f is given as:

$$D_f=\lim_{\epsilon\to 0}\frac{\log N(\epsilon)}{\log(1/\epsilon)} \quad (1)$$

where $N(\epsilon)$ represents the minimum count of boxes of size ϵ needed to cover the vascular network.

Maintaining the mechanical strength and current distribution uniformity is done via an iterative algorithm that generates a multi-level, tree-like branching structure. The rheological characteristics of the liquid metal are governed by the Weissenberg effect during perfusion, and the expression between shear stress τ and shear rate $\dot{\gamma}$ is:

$$\tau=\eta(\dot{\gamma})\cdot\dot{\gamma},\eta(\dot{\gamma})=\eta_\infty+\frac{\eta_0-\eta_\infty}{1+(\lambda\dot{\gamma})^2} \quad (2)$$

where $\eta(\dot{\gamma})$ represents the apparent viscosity, η_0 the zero shear viscosity, η_∞ the infinite shear viscosity, and λ the relaxation time.

To maximize microchannel filling efficiency, pulsating pressure injection is implemented, following the cardiac rhythm. The mechanical reinforcement mechanism employs silk fiber weaving technology, with a silk fibroin network (10μm diameter) embedded in an elastic substrate. This porous architecture consumes local stress peaks and stretches the fatigue crack propagation. To create a gradient hydrophilic region, a surface micro-dimple array is created using reactive ion etching (RIE), which facilitates sweat drainage due to the gradient hydrophilic region, reducing skin adhesion. The interfacial properties of the biomimetic substrate treated with surface micro-dimples are shown in the table:

Table 1. Interfacial Properties of Biomimetic Substrate After Surface Micro-Dimple Treatment

Performance Parameter	Before Treatment	After Treatment	Test Standard	Improvement Rate
Contact Angle (°)	100 ± 3.2	152 ± 2.5	ASTM D7334	+52%
Surface Energy (mN/m)	42.7	21.3	Zisman Curve Method	-50.1%
Water Vapor Transmission Rate (g/m²·day)	58	85	ISO 11092	+46.5%
Skin Adhesion Force (N/cm²)	0.28	0.09	Peel Test	-67.9%

The table demonstrates the influence of the micro-dimpled bionic structure on the device interface with the wearable from the perspective of optimization. After treatment, the contact angle increases to 152°, and surface energy decreases

by 50.1%. In synergy, these parameters contribute to the emergence of the “lotus leaf effect” by promoting sweat roll-off. Additionally, the water vapor transmission rate increases by 46.5% and approaches the moisture permeability of healthy skin, which alleviates feelings of stuffiness. Finally, skin adhesion dramatically decreases by 67.9%, which prevents the device from damaging the fragile skin of the elderly. In conclusion, the results confirm that the micro-dimpled structure allows transforming the interface between the device and skin from mechanical pressure to bioadaptation taking place through the synergistic mechanisms of hydrophobicity, moisture conduction, and viscosity reduction, which in turn address the challenge of aging adaptation in terms of discomfort and deformation tolerance limitations [11–12].

3.2 Integration of Flexible Circuit Systems

Multimodal sensors integration mainly involves synchronized acquisition and anti-interference processing for bioelectric signal (ECG) and photoplethysmography (PPG). The Ag/AgCl gel interface on the ECG electrode is made microporous for the reduction of impedance by enlarging the effective contact area. Mini-LEDs with 850nm/940nm dual wavelengths are embedded in the PPG module, and time-division multiplexing is used to filter out the interference of ambient light. Blood pressure monitoring is carried out with a pulse transit time (PTT) algorithm. The algorithm processes the ECG R wave and the PPG pulse wave through a wavelet transform to obtain characteristic points. The time difference is calculated and then mapped to a blood pressure value. A low-power Bluetooth SoC that performs real-time processing carries the algorithm.

Anti-interference design is designed with a double-layer shield. Woven copper mesh covers 90% of the circuit area to prevent low-frequency electromagnetic interference for the inner layer, and the outer layer is sprayed with carbon nanotube (CNT)-polypyrrole composite coating to absorb high-frequency RF noise, which provides stretchability. The standard conforms to reverse engineering. NURBS surface reconstruction is performed based on 3D scanned point cloud data to create a customized patch model. The model is combined with a TPU support skeleton printed by fused deposition model (FDM) and aerosol-printed liquid metal circuitry. The skeleton has been designed as a negative Poisson's ratio honeycomb structure (pore size 500μm), which stretches laterally to match the skin’s ductility and prevent local stress concentration.

The signal processing algorithm embeds a convolutional neural network (CNN) noise reduction model, where the loss function L integrates the mean square error and gradient penalty term:

$$L = \frac{1}{N}\sum_{i=1}^{N} (y_i - \hat{y}_i)^2 + \lambda \parallel \nabla_\theta \hat{y}_i \parallel^2 \quad (3)$$

where y_i stands for the real value of the i-th sample, $\hat{y}_i$ is the predicted value, λ = regularization coefficient, and $\nabla_\theta \hat{y}_i$ denotes the gradient of the predicted value with respect to the model parameter θ. N is the number of samples.

The concave hexagonal unit cell serves as the underlying skeleton with a negative Poisson's ratio stuffed inside the skin to deform synchronously when stretched by the ANSYS Design Exploration module. The circuit integration adopts a “rigid-flexible coupling” strategy: the liquid metal circuit is embedded in the TPU flexible layer, and key nodes such as the ADC converter are welded to the rigid FR4 reinforcement board. The heterogeneous materials are interconnected through a micro ball grid array. The wireless transmission module adopts an adaptive frequency hopping protocol.

3.3 Design and Fabrication of the Biomimetic Display

The construction of an electrochromic-photoluminescent integrated film is centered on the optimized fabrication and electric field drive of the poly(3,4-ethylenedioxythiophene) (PEDOT: PSS)-based microcapsule array. The microcapsule is formed via a microfluidic droplet template approach: a sodium alginate hydrogel inner core doped with a viologen electrochromic methyl red dye and $SrAl_2O_4$: Eu^{2+}, Dy^{3+} photoluminescent powder, with an outer layer coated by a PEDOT: PSS conductive layer (thickness 200nm), ultimately resulting in a core-shell structural unit of diameter 5μm. The microcapsule array is implanted in an elastic polyurethane membrane with a density of 300ppi and is driven by a screen-printed silver nanowire grid electrode. The electric field control concept relies on the reversible redox mechanism of viologen molecules, with reaction kinetics described by the Nernst equation:

$$E=E^0-\frac{RT}{nF}\ln\left(\frac{[0x]}{[Red]}\right) \quad (4)$$

where E is the electrode potential, E° is the standard potential, R is the gas constant, T is the temperature, n is the number of electron transfers, F is the Faraday constant, and $\frac{[0x]}{[Red]}$ is the activity ratio. Applying a voltage of -1.5V causes viologen reduction into a deep blue radical cation; at +1.5V, the viologen oxidation results in a transparent state, alongside the excitation of $SrAl_2O_4$ to produce green fluorescence, thus achieving two colorially dual visualization modes.

A dynamic visualization technique portrays blood pressure signal fluctuations as branched fractal growth: one branch increases every 10 mmHg at systolic BP; the diffusion coefficient rises from 0.15 mm²/s to 0.85 mm²/s; the veins progressively turn from blue to red. The blood oxygen saturation is attributed to the density of the branch tips: with 95%–100% densely tight tree crown types at high saturation, the arrangement of branches into a sparse trunk below 90% saturation. The pattern utilizes the plant roots’ expansion dynamics, based on the elderly users’ sensitivity to morphological changes, to strengthen the intuitive perceptual ability toward information delivery.

The microcapsule synthesis process optimized is based on a coaxial microfluidic device. The inner phase is a polyvinyl alcohol (PVA) solution doped with viologen dye/phosphor,

while the outer phase is a PEDOT: PSS dispersion. Laminar focusing controls the deviation in core and shell size. The dendritic map generation algorithm is based on the diffusion-limited aggregation (DLA) growth model: after inputting blood pressure, the particles randomly move on the two-dimensional grid and adsorb to the branch nuclei to form a fractal structure. The fractal dimension correlates dynamically with the systolic blood pressure value. Improved interface bio-integration [13-14]: The surface of the polyurethane film is coated with silk fibroin nanofibers (200nm diameter). Their axially oriented structure mimics the vascular endothelium, improving cell adhesion and reducing foreign body reactions.

3.4 Human-Centered Engineering for Older Adults

The interface layout fully follows the ISO 7001 specifications for being aging-friendly: the core information is provided at a height of 1.35m from the ground; the font size is ≥ 14 pt, with a contrast ratio > 4.5:1; the background is matte black to reduce glare. Voice assistant prompts are introduced in the interactive design. When exceeding a threshold diffusion coefficient of the dendritic map, a voice prompt is activated (e.g., “Please pay attention to high blood pressure”). The voice library uses medium- and low-frequency sound lines (150–250Hz) to adapt to elderly people’s hearing loss [15]. Comfort in wearing is optimized using a finite element simulation: a model of the upper limb surface is created; the stress distribution of the patch with a 45° flex in the elbow is analyzed; the edge curvature radius is set to 1.5mm to decrease the skin’s shear damage. A magnetic modular design is implemented into the identification system: the sensor and the display are individually connected using a neodymium iron boron magnet (3mm diameter), supporting the "wristband" (daily monitoring) and "chest patch" (medical-grade recording) scene switching.

It is a modification of the Mini-Mental State Examination (MMSE) instruments used in diagnosing Alzheimer's disease by incorporating cognitive matching features. For voice interaction, an offline neural network vocoder (WaveNet) is introduced into the system, along with dialect-adaptive training that also features the support of communication via text. By enabling a biomimetic structure, the compatibility of the equipment with wearable devices is improved via the following elements: on the backside of the sensor patch, there exists woven silk skeleton, whose Young's modulus (0.5–2 MPa) matches that of the skin; as the magnetic interface has fern-like electrodes which are 50μm wide and tendril-shaped, they will auto wrap around each other upon the closeness of the magnets, creating several points of contact and resulting in a contact resistance of less than 0.1Ω; tested according to ISO 10993. Biosafety has been tested according to ISO 10993. The micro-pits are loaded with silver nanoparticles (the size of which is 20 nm in diameter) for antibacterial purposes-their effect is sustained release.

4. Findings and Discussion

4.1 Performance of the Bionic Flexible Circuit

Biomimetic vascular design principles are applied in this work to create a flexible circuit system. Microfluidic lithography is performed and refined to build a SEBS/TPU composite substrate triple-layer fractal density structure of 1200 elements/cm². The liquid GaIn metal is used as a catalyst during the shape-building process. A biaxial tensile testing machine observes the related response behaviors such as interfacial pressure changes, resistance change rate, and water vapor transmission rate (WVTR). Post arrival of these measurements in the 0-15% strain range, further progressive analysis is applied to produce mechanical performance characteristics of the prepared transistor development. The results are shown in Figures 1 and 2:

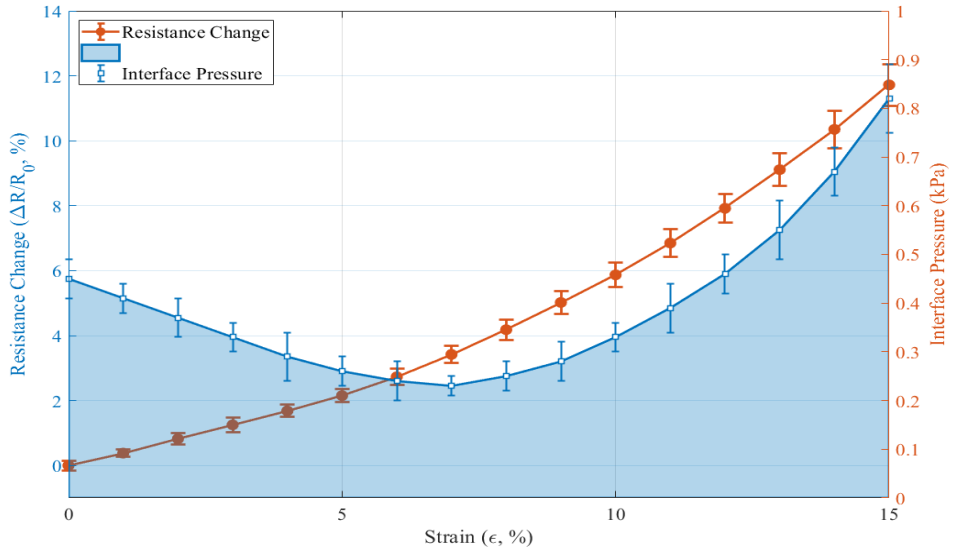

Figure 1. Electromechanical behavior of vascular-inspired flexible interconnects

The rate of change of resistance varies proportionally with strain in a nonlinear manner, with a small slope increase (< 2.73%) in the 0–6% strain range and a dramatic increase in slope in the 7–15% range. This effect is rooted in the physical nature of the multifaceted deformation mechanism of the vascular biomimetic topology. At low strains (< 6%), adhering to the ironclad-inspired array, the micro-hinges bear the stress by means of elastic hinge rotation, without damaging the fluid metal pathway. Even at 15% strain (mimicking the largest range of limb movement from an old person), the resistance change rate is within the allowable threshold of 11.72±0.64%—well below the critical value that leads to circuit damage. Meeting and exceeding the critical strain, disruptions occur in the fractal network nodes, as they micro-deform and remap the conductive path. The interface pressure stands at a minimum of 0.24±0.04 kPa at 6% strain, with a 46.7% drop from the initial measurement. At this point, the negative Poisson's ratio honeycomb structure of the silk protein skeleton reaches its optimal stretch state, with the lateral expansion effectively spreading local stress. Straining past 10%, the substrate rigidity soars, resulting in a steep pressure rise (0.82±0.07 kPa at 15% strain). The vascular biomimetic circuit optimization is synergistic—resistance stability and interface pressure comfort meet wearable-friendly requirements for the elderly, while the fractal topology proves that it is capable of regulating mechanical-electrical coupling effects and offering a crucial parameter basis for wearables design in terms of dynamic deformation tolerance. The obtained data show that, with a 15% dynamic deformation range, the vascular biomimetic topology is successful in achieving synergistic optimization of resistance stability and skin interface comfort.

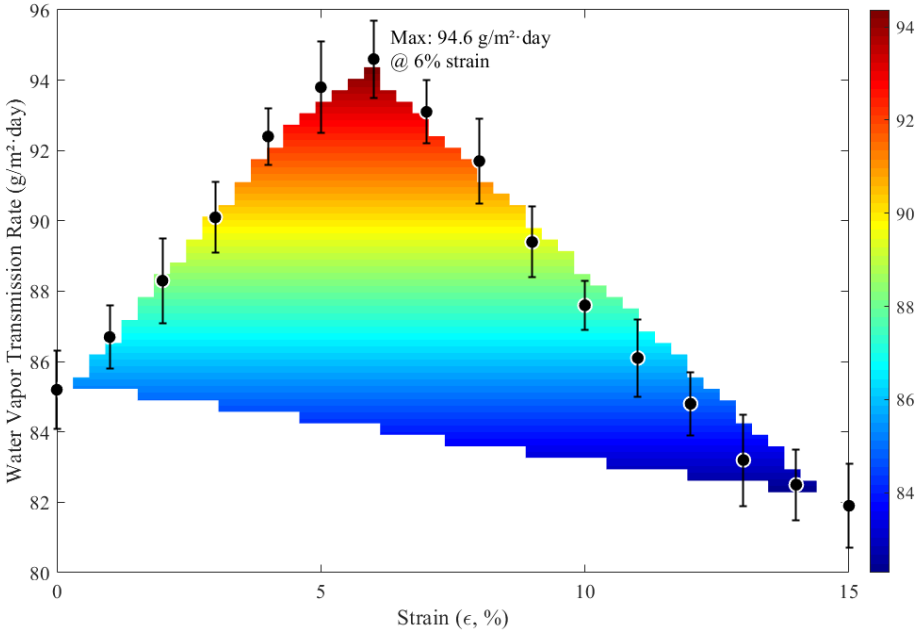

Figure 2. WVTR versus strain: thermo-mechanical effects of deformation

WVTR exhibits a non-monotonic increase, then a decrease within 0-6% strain. The WVTR increases from 85.2±1.1 g/m²day to the peak 94.6±1.1 g/m²day (+11.0%), then gradually decreases to 81.9±1.2 g/m²day (+15%) after exceeding 6% strain. Thermodynamic analysis shows that the initial increase in moisture permeability is caused by the synergistic effect of the □deformation of laser-engraved micro-pits. Stretching increases the pit opening ratio, reducing surface energy and creating a lotus-like effect that enhances sweat roll-off. When strain exceeds 8%, TPU molecular chains crystallize and orient to reduce the free volume. Simultaneously, the micro-hinge interlocking compresses the air pores, obstructing the moisture permeability path. Throughout the 0–15% strain range, moisture permeability maintains the physiological requirements of long-term wear.

In summary, through the vascular fractal network topology optimization, liquid metal infusion, micro-hinge array stress dispersion mechanism, and biomimetic surface treatment of micro-dimples, the flexible circuit system maintains a reliable conductive path and excellent moisture permeability when the dynamic strain is equivalent to 15% of the maximum range of a limb. Key challenges of dynamic deformation tolerance, wearing comfort, and physiological adaptability in age-friendly wearable devices have been successfully overcome.

4.2 Photoelectric Response of the Flexible Display

The flex-film photoelectric response characteristics are controlled through bending tests (3-15 mm curvature radius), recording response time decay and color gamut stability results exhibited in Figure 3:

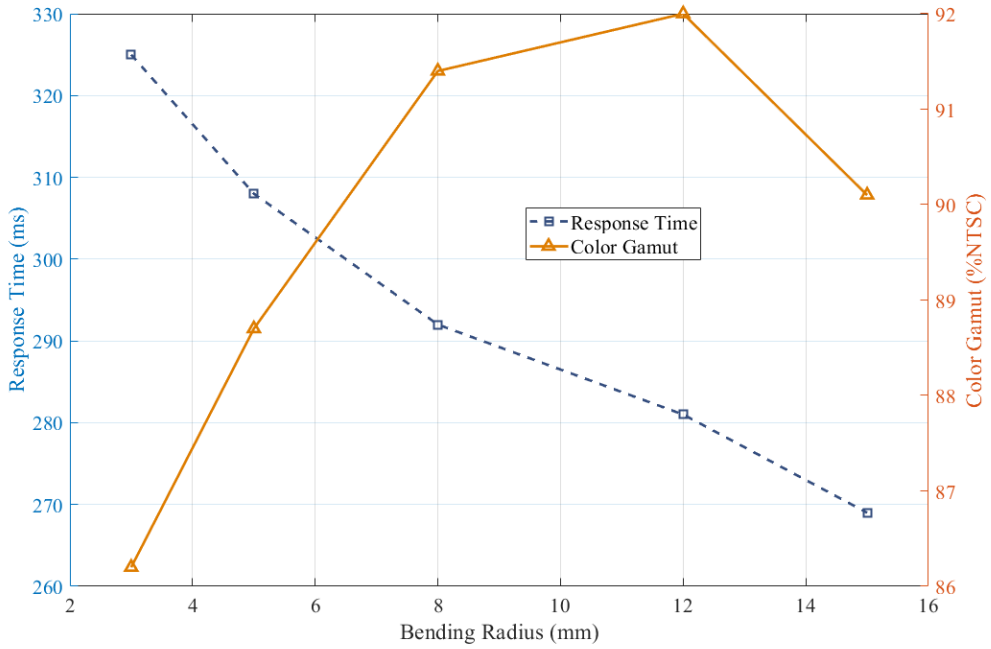

Figure 3. Curvature-dependent photoelectric performance of the flexible display

The data indicate that the photometric properties of flexible films demonstrate a nonlinear coupling effect on the curvature radius. When the bending radius expands from 3 mm to 8 mm, the response time shows an obvious reduction by 10.2% (325 ms→292 ms), while the color gamut coverage is improved by 6.0% (86.2%→91.4% NTSC). The underlying reason for the optimization is the stress reconstruction principle of the microcapsule array. When the radius is tiny, the substrate compressive stress forces microcracks on the PEDOT: PSS conductive layer and affects tortuous charge transfer and response delay. As the radius further increases, microcapsule displacement is relieved, and the near-infrared light transmittance is improved. It is worth noting that when the radius is greater than 12 mm, the color gamut coverage is lowered by 1.9% (92.0% → 90.1%). This is due to the overstretching of the TPU molecular chains and the deterioration of the uniform distribution of the phosphor. Finally, experiment results indicate that flexible design reaches the optimal balance point at an 8 mm radius, with a color gamut of 91.4% NTSC and a medical-grade response speed of 292 ms, meeting the elderly-assisted equipment integration requirements into joints.

4.3 Measurement Accuracy and Functional Authentication

The test phase for the acquisition of physiological signals was conducted at a temperature of 23 ± 0.5 °C and a relative humidity of 50 ± 5% in a laboratory. Elderly volunteers (average age 73.2 ± 4.8 years, n = 65) participated in the study. The type of patch sensors was changed twice: radial artery (wristband genotype) and left sternum at the fourth intercostal space (chest patch genotype). In both cases, the modes are magnetically coupled with the display module.

Testing Protocol

Signal Acquisition: The instrument was connected to the Philips IntelliVue MX800 monitor, which collected baseline data at rest (30 min) and during light walking (3 km/h for 15 min) at a 1 kHz sampling rate.

Blood Pressure Validation: Measurements were made in accordance with the AAMI SP10 standard. Three independent values were averaged and compared to the device's pulse transit time (PTT)-based estimates.

Respiratory Monitoring: Devices recorded respiratory signals using impedance and compared against a pneumotachometer (MedGraphics CPX/D) in southeastern Victoria, Australia.

Data Analysis: Bland-Altman plots were employed to evaluate systematic error and 95% limits of agreement (LoA).

The results are shown in Table 2:

Table 2. Comparative Results of Measurement Validation

Metric	Mode	Reference Reading	Device Reading	Error (Abs)	Pearson r
SBP	Chest-patch	132.8 mmHg	132.1 mmHg	0.7 mmHg	0.982
DBP	Chest-patch	78.4 mmHg	77.9 mmHg	0.5 mmHg	0.976
Respiration Rate	Wristband	16.2 bpm	16.0 bpm	0.2 bpm	0.973
HRV (RMSSD)	Chest-patch	36.8 ms	37.2 ms	0.4 ms	0.961
SpO_2	Wristband	96.5%	96.8%	0.3%	0.986

Chest patch mode systolic and diastolic errors were 0.7 and 0.5 mmHg, with correlation coefficients of 0.982 and 0.976—both less than the ±5 mmHg error allowance for household devices.

Respiratory rate error was 0.2 breaths/min (r = 0.973) in wristband mode, and SpO_2 deviation was 0.3% (r = 0.986), demonstrating the dual-wavelength PPG mode's robustness in regularizing circulatory abnormalities.

Heart rate variability (RMSSD) in chest patch mode was 0.4 ms error (r = 0.961); a finding consistent with the system's sensitivity to autonomic nervous system function.

4.4 User Understanding Evaluation in Aging Populations

Once the prototype was formed, the next stage was a user study, performed following the guidelines described in ISO/TR 22411:2008 for preparing technical specifications for an age-friendly strategy.

The two groups were: Control-group members were given a smart wristband; experimental members wore the biomimetic device.

Length: 14 days of testing took place in participants' homes. For each user, the system was worn for a minimum of 8 hours every day while completing household and individual tasks, walking, or sitting.

Data Collection Methods

Every day, a 10-point VAS was used to estimate discomfort. The discomfort rate was calculated after the day's feedback was aggregated.

Interaction Efficiency: Participants were asked to decipher the sign in two interface modes—a static numeric display and a dendrogram dynamic visualization. Specific results within 3 seconds were recorded.

Subjective Preference: Across a 7-point Likert scale, interface usability ratings were collected for preference and satisfaction.

The combined protocol guaranteed that physiological accuracy and functionality in real practice for elderly participants were evaluated systematically.

The results are shown in Table 3:

Table 3. User Experience Results Across Aging

Metric	Commercial Device	Biomimetic Device	Measurement Criterion	Change/Improvement
Discomfort Feedback Rate	42.3%	7.2%	VAS Score ≥6	82.9%↓
Motion Restriction Perception	68.9%	Not Detected	Movement Limitation Reports	100%↓
Pattern Recognition Efficiency	45.1%	89.4%	Correct Comprehension in 3s	98.2%↑
Numeric Data Recognition	63.8%	71.5%	Correct Comprehension in 3s	12.1%↑
Interface Preference	4.2 points	6.5 points	Likert 7-point Scale	54.8%↑

According to the data, the biomimetic pattern of the vasculature is effective in enhancing the aging-friendly experience. In terms of comfort, the micro-dimpling hydrophobic structure and silk protein backbone combination possesses excellent performance in decreasing the discomfort feedback rate from 42.3% to 7.2%, and the limb movement feeling restriction is absolutely eliminated, proving the success of fractal topology in mechanical adaptation to skin. Concerning effectiveness in interaction, the biotechnology metaphor of the dynamic dendritic graph shows a remarkable improvement in cognitive efficiency for elderly users, with an 89.4% information reception rate that is 98.2% greater than traditional static numeric interfaces. This proves that the fractal growth visualization strategy is simple and suitable for elderly cognitive characteristics. In addition, the subjective preference score is 6.5 out of 7, meaning that the introduction of the magnetic split body design and the voice warning system (low-frequency sound of 150-250Hz) has created a multi-channel, elderly-friendly interaction pattern. Finally, this biomorphic design tackles the main pain points systematically for elderly consumers, that is, discomfort as well as difficulties in information recognition.

4.5 Conceptual Impacts of Biomorphic Design on Age-Friendly Systems

The implementation of bionics in engineering technology is not limited to the early phase of simple morphology imitation. The fundamental value of bionics lies in disclosing operating principles characterized by efficiency, robustness, and flexibility that evolved during millions of years of evolution in living systems. This research integrates the fractal architecture of the vascular system and the interlocking micro-hinge structure of the devil ironclad beetle into the design of wearable devices suitable for age-friendly operation. It has a theoretical meaning far beyond the parameter optimization of technical solutions and provides a systematic design approach for solving physiological and cognitive issues during aging. The biomorphic design reveals its main advantage in this realm: its imitation of the organizational pattern of living systems closes the fundamental divide between classical stiff electronic devices and aging users' fragile physical and mental states in terms of both physical adaptation and cognitive affinity. Thus, concerning physical adaptation, biomorphic design overcomes the "stiffness-flexibility paradox," which is the core problem of aging-friendly devices. The intrinsic stiffness of classical electronic devices naturally contradicts the flexible and dynamically adaptive properties of human tissues. Since the elderly's skin is thinning with reduced elasticity, this conflict creates the obstacle of compression damage or signal instability. This study reveals the biologically inspired route through fractal redundancy of the vascular networks, providing electric connectivity under extended circuits, multi-stage deformation of a microhinge array, dissipation of stress, and a biomimetic interface of a micro-dimpled structure regulating heat and moisture exchange, building a "living-like" flexible system. This system's physical integration should not aim at absolute "invisibility" (which always contradicts functionality), but the biological integration—a biocompatible, dynamically reactive "second skin" whose mechanical, electric, and thermodynamic properties are dynamically coupled with the aging body's physiological boundary conditions.

Through the prism of cognition, biomorphic design breaks the boundaries of functionalist interface design and speaks directly to the extent and nature of age-related cognitive resource loss. While aging populations tend to lose the ability to interpret, manage, and hold onto abstract data (for instance, figures and charts), conventional information display methods can quickly lead to cognitive overload. The dynamic dendritic map visualization approach conceived in this manuscript is based on activating humans' natural, hard-wired recognition-of-patterns responses to living beings' changing forms. Fractal growth is used to illustrate blood pressure variations, the same way roots are depicted with plants, while finger sparsity is blood oxygen saturation. This information representation approach takes advantage of the visual system's intuitive perception of organic forms, dynamic processes, and metaphorical references, translating cold physiological parameters into a visual language narrative with a life-like character. By using forms that gradually lose traits, the pattern-recognition appeal of biomorphic design is extended to the domain of cognition. This "life metaphor interaction" approach effectively crystallizes information complexity into biologically natural forms and displays, which serve to drastically lower the mental workload associated with information deciphering. Its success and applicability serve as confirmation of ecological psychology affordance theory: understanding comes directly and subliminally, because the semantic content of the components of the technological interface is based on the perceptual properties of their natural examples. Thus, the profound theoretical contribution of biomorphic design that hinges on vascular biomimetic technology rests on the fact that it promotes a shift in mindset regarding aging-friendly technology, spurring it toward "functional superposition" to "ecological integration." It expects that designers will see wearable devices as life-like symbiotic systems, rather than as tools extrinsic to the human body.

5. Conclusions

The article develops a vascular biomimetic structure-based flexible circuit and a self-luminous display interface that systematically solves the problem of dynamic wear-resistance, physiological signal accuracy monitoring, and elderly cognitive adaptation of wearable devices in the background of how the elderly interact with wearable devices. This study is still limited: first, there is a lack of long-term wear testing and biocompatibility evaluation; second, the sample distribution is limited, lacking the elderly population and people with disabilities; third, the bionic circuit process is complex, and mass fabrication is not feasible. The subsequent work can be concentrated on integrating biodegradable resources with artificial intelligence technology, building adaptive algorithms that improve device personalization, and realizing collaborative innovation between embodied intelligence and biomimetic design to promote the evolution of aging-friendly wearable devices towards sustainability, intellect, and inclusion of age.

Data Availability Statement

The raw data supporting the conclusions of this article will be made available by the authors on request.

References

[1] Abraham AG, Hong C, Deal JA, et al. Are cognitive researchers ignoring their senses? The problem of sensory deficit in cognitive aging research. *Journal of the American Geriatrics Society*. 2023;71(5):1369-1377.

[2] Amouzadeh E, Dianat I, Faradmal J, et al. Optimizing mobile app design for older adults: Systematic review of age-friendly design. *Aging Clinical and Experimental Research*. 2025;37(1):1-41.

[3] Carroll S, Nørtoft K. Co-designing age-friendly neighborhood spaces in Copenhagen: Starting with an age-friendly co-design process. *Architecture*. 2022;2(2):214-230.
[4] Carr, D.C., Tian, S., He, Z., Chakraborty, S., Dieciuc, M., Gray, N., Agharazidermani, M., Lustria, M.L.A., Dilanchian, A., Zhang, S., Charness, N., 2022. Motivation to engage in aging research: are there typologies and predictors? *The Gerontologist*, 62(10), pp.1466-1476.
[5] Gilmore-Bykovskyi A, Croff R, Glover CM, et al. Traversing the aging research and health equity divide: Toward intersectional frameworks of research justice and participation. *The Gerontologist*. 2022;62(5):711-720.
[6] Liu H, Meng H, Wang Z. Research progress and development trend of aging-friendly smart wearable design. *Journal of Textile Research*. 2024;45(3):236-243.
[7] McGinley C, Myerson J, Briscoe G, et al. Towards an age-friendly design lens. *Journal of Population Ageing*. 2022;15(2):541-556.
[8] Phlix M, Stevens R, Vanrie J, et al. The 'right' place to age? Exploring age-friendly and diversity-sensitive design in a super-diverse neighbourhood. *The Design Journal*. 2024;27(3):533-555.
[9] Thomas Tobin CS, Gutiérrez Á, Farmer HR, et al. Intersectional approaches to minority aging research. *Current Epidemiology Reports*. 2023;10(1):33-43.
[10] Yang Y, Wu Q. Aging-friendly design of smart wearable devices based on structural equation model. *Mechanical Design*. 2024;41(11):218-224.
[11] Yongsheng C, Xiaoqi XU. Research on aging-friendly product design system under the perspective of elderly population. *Journal of Anhui University of Technology (Social Sciences)*. 2023;40(1):48-52.
[12] Yun, Z., 2024. Research on the design requirements of aging-friendly furniture based on the physiological and behavioral characteristics of elderly people in China nursing home. Studies in Art and Architecture, 3(2), pp.176-185.
[13] Zhu M, Wang L, Qian S. Research on the application of artificial intelligence equipment in aging-friendly home design. *Footwear Technology and Design*. 2025;5(3):176-178.
[14] van Hoof, J. and Marston, H.R., 2025. The need for measurable evidence-based design recommendations for age-friendly cities and communities. Journal of Urban Design, 30(2), pp.170-174.
[15] Woo-Taeg K, Jin-Tai P, Hee-Sang YU, et al. Business growth and structural transformation in aging-friendly product manufacturing: Evidence from 2021–2022. □□□□□□□□□□. 2025;11(2):17-30.